

# Fabrication of carbon fiber supported zirconium–titanium nanocomposites for efficient photocatalytic decolorization of Orange II dye under visible light irradiation

Esra Bilgin Simsek<sup>1</sup>  · Pelin Demircivi<sup>1</sup> · Dusan Berek<sup>2</sup> · Ivan Novak<sup>2</sup>

Received: 21 August 2017 / Accepted: 24 November 2017 / Published online: 2 December 2017  
© Akadémiai Kiadó, Budapest, Hungary 2017

**Abstract** A series of carbon fiber based  $ZrO_2$ – $TiO_2$  (Zr/Ti/CF) nanocomposites were synthesized with carbon fiber loadings from 3 to 10 wt% by the solvothermal method. For comparison, Zr/Ti, Ti/CF and Zr/CF catalysts were also synthesized. The resultant samples were characterized by SEM, XPS, XRD, FT-IR, and UV–Vis spectroscopy. XRD results revealed that the catalysts were having anatase  $TiO_2$  with excellent crystallinity. SEM studies show that the surface of Zr/Ti/CF/10 catalyst has round-shaped grains with dimensions in the range of 16–20 nm. Under UV-A and visible light irradiation, Zr/Ti/CF catalyst exhibited excellent photocatalytic performance for Orange II degradation when compared with Zr/Ti, Zr/CF and Ti/CF. The enhancing efficiency was attributed to the synergetic effect of adsorption–photocatalysis and to the reduction of the band gap energy.

**Keywords** Carbon fiber · Zirconium ·  $TiO_2$  · Photocatalytic degradation · Orange II

---

**Electronic supplementary material** The online version of this article (<https://doi.org/10.1007/s11144-017-1320-x>) contains supplementary material, which is available to authorized users.

---

✉ Esra Bilgin Simsek  
esrabilgin622@gmail.com; ebilgin.simsek@yalova.edu.tr

<sup>1</sup> Department of Chemical and Process Engineering, Faculty of Engineering, Yalova University, 77100 Yalova, Turkey

<sup>2</sup> Polymer Institute, Slovak Academy of Sciences, 84541 Bratislava, Slovakia

## Introduction

In recent years,  $\text{TiO}_2$  photocatalyst has been extensively utilized in the photocatalytic degradation of organic pollutants. However, the photocatalytic activity of  $\text{TiO}_2$  is partly limited by fast charge-carrier recombination and due to a large band gap ( $\sim 3.2$  eV for anatase phase), which restricts the use in practical applications [1, 2]. In order to improve the photocatalytic activity of  $\text{TiO}_2$ , a tremendous number of studies have been carried out by co-doping with a metal [3] or non-metal [4], and fabrication of composites with other materials [5, 6]. The transition metal ions could act as electron traps, which improve the efficiency of charge transfer [7]. The introduction of metal atoms into the  $\text{TiO}_2$  lattice also extends the light absorption into the visible region (400–800 nm) [3]. Due to its approximately similar electronegativity and ionic radius of  $\text{TiO}_2$ , zirconium ( $\text{ZrO}_2$ ) is a promising candidate for the doping [1]. According to the studies in literature, it was shown that doping of Zr into  $\text{TiO}_2$  structure improves photocatalytic activity of  $\text{TiO}_2$  [8, 9].

However,  $\text{TiO}_2$  and  $\text{ZrO}_2$  powders can be inconvenient for the industrialization considering their separation and recovery from water in a slurry system after the photocatalytic reaction [10–12]. An ideal way is to grow photocatalysts onto solid surfaces in order to improve both photocatalytic performance and repeating circles. Carbonaceous materials could provide one of the approaches to address the issue of separation and recovery of nanosized semiconductors. They can also provide an enhancement in the photodegradation activity via the synergetic effect of adsorption–photocatalysis. The incorporation of carbon also enables additional band gap states in the electronic structure and shifts the absorption band to visible region [13]. Carbon fibers belong to the group of highly microporous carbon materials, they have a higher surface area, large pore volume and uniform micropore size distribution [6, 10]. Moreover, the intrinsic properties of high adsorption capacity and superior mechanical strength also make them equally important in environmental remediation [11, 14]. Li et al. [12] fabricated carbon fiber supported  $\text{TiO}_2$  and found that the composite catalyst showed high activity for the acid orange 7 degradation. Wang et al. [11] observed that  $\text{TiO}_2$ -loaded CFs exhibited the best photocatalytic performance for methyl orange degradation.

Although carbon fiber based  $\text{TiO}_2$  catalysts have been synthesized [6, 10–12], on the basis of our research, the immobilization of co doped  $\text{TiO}_2$  on CF has been investigated for the first time in this study. Herein, carbon fiber based Zr– $\text{TiO}_2$  (Zr/Ti/CF) nanocomposites were synthesized with carbon fiber loadings from 3 to 10 wt % via in situ process by the solvothermal method. The photocatalytic performances of the synthesized nanocomposites were tested by performing degradation experiments with Orange II dye under UV-A and visible light irradiation.

## Materials and methods

### Materials

All the chemicals were of analytic grade and used directly without further purification. For the preparation of the microporous carbon fibers (CF), the delignified cellulose microfibrils from pulp factory Hencovce, Slovakia, was used as the starting material.

### Synthesis of carbon fiber based Zr–TiO<sub>2</sub> catalysts

Raw carbon fibers were prepared according to the procedure as described in our previous study [15]. Briefly, the cellulose microfibrils were placed into a stainless steel vessel provided with a slightly sealed lid and carbonized in an oven at 700 °C for 1 h in the absence of air oxygen.

Carbon fiber based Zr–TiO<sub>2</sub> (Zr/Ti/CF) nanocomposites were synthesized with carbon fiber loadings from 3 to 10 wt% via an in situ process by the solvothermal method. Initially, 0.5 g of ZrOCl<sub>2</sub>·8H<sub>2</sub>O and 20 mL of tetrabutyl titanate was stirred in solution containing 40 mL of ethanol for 1 h (Solution I). Another solution was prepared by defined amount of CF (10 wt% with respect to Zr–Ti) in 30 mL of ethanol with ultrasonication for 1 h which results CF suspension (Solution II). Solution I was added dropwise to Solution II under vigorous stirring at room temperature. To the resultant mixture, another solution containing 2 mL of HCl and 4 mL of H<sub>2</sub>O was added dropwise from the burette under stirring. The resultant colloidal suspension was stirred for 1 h and the gel was aged for overnight. Then, the gel was operated by hydrothermal treatment in a Teflon-lined stainless steel autoclave at 180 °C for 12 h. The products were cooled at room temperature, washed with de-ionized water and ethanol, dried and calcined at 500 °C for 2 h. The resultant powder labelled as Zr/Ti/CF/10 (10 wt% of CF). By following the same procedure, Zr/Ti/CF/3 and Zr/Ti/CF/5 were prepared by taking 3 and 5 wt% CF suspensions, respectively. For comparison, Zr doped TiO<sub>2</sub> (Zr/Ti) without CF content, Ti/CF (10 wt% of CF) and Zr/CF (10 wt% of CF), were synthesized by the same method.

### Characterization of catalysts

The surface morphology of the nanostructures on each prepared sample was analyzed by scanning electron microscopy and energy dispersive X-ray spectroscopy (Philips XL30 ESEM-FEG/EDAX). The crystal structure was analyzed using X-ray diffraction (XRD; Rigaku D/Max-IIIIC diffractometer) with 1.54 Å Cu K<sub>α</sub> radiation and a 2θ range of 10–80°. UV–Vis absorption measurements were carried out using a Perkin-Elmer UV–VIS Lambda 2S spectrometer. The Fourier transform infrared (FTIR) spectrum was recorded by a Perkin Elmer Spectrum One instrument using attenuated total reflectance method, in the wavenumber range of 600–4000 cm<sup>-1</sup>. The surface composition of the samples was investigated using

X-ray photoelectron spectroscopy (XPS; Thermo Scientific K-Alpha X-ray photoelectron spectrometer), which is capable of providing atomic and molecular information on the surfaces of materials.

### Photocatalytic degradation studies

Photocatalytic degradation studies were conducted under two light sources. A column-shaped stainless steel cabinet equipped with 18 UV lamps were used for UV-A light ( $\lambda_{\text{max}} \sim 365$  nm) experiments. A square-shaped reactor donated with two visible metal halide lamps ( $\lambda$ : 400–800 nm) were used to offer visible light irradiation. The system is cooled through a fan at the bottom of the cabinet. For each degradation experiment, Orange II solution with concentration of 10 mg/L was prepared in 50 mL double distilled water at neutral pH. Before the photocatalytic experiments, the solution was stirred for 30 min in dark to establish adsorption equilibrium. Aliquots (5 mL) were collected at defined time intervals and filtered with 0.45  $\mu\text{m}$  syringe membrane filters. In order to examine the adsorption performance of catalysts, degradation experiments were also conducted in the absence of light. Orange II decolorization was monitored by UV–Vis spectra at 485 nm.

In order to examine the chemical stability of the as-prepared Zr/Ti/CF, the catalyst was recycled and reused five times for the decomposition of Orange II. After each cycle, the solution was centrifuged, washed by deionized water, and then re-injected into fresh solution for the next cycle.

In order to confirm the reproducibility of the results, all degradation experiments were carried out with duplicated runs for each condition, and the experimental error was calculated to be within  $\pm 5\%$ .

## Results and discussion

### Catalysts characterization

The morphologies of Zr/Ti and CF based catalysts were observed by SEM and were shown in Fig. 1. The surface of Zr/Ti has a round-shaped grain texture and the particle size was in the nanometer range. The morphology images after carbon fiber incorporation shows that the  $\text{TiO}_2$  and  $\text{ZrO}_2$  based catalysts still have similar structure. The surface of Zr/Ti/CF/10 catalyst has round-shaped grains with dimensions in the range of 16–20 nm.

The crystal phase composition of Zr/Ti and Zr/Ti/CF/10 catalysts is obtained by XRD analysis (Fig. S1a). No diffraction peaks of  $\text{ZrO}_2$  were evident as Zr reactant was used as 5% wt. of  $\text{TiO}_2$  in the preparation of samples. The XRD pattern of raw  $\text{TiO}_2$  catalyst is found as well developed anatase phase at  $25.30^\circ$ ,  $37.50^\circ$ ,  $48.10^\circ$ . The major peak at  $29.10^\circ$  was observed for raw  $\text{ZrO}_2$ , which indicates the tetragonal  $\text{ZrO}_2$  crystal phase. No diffraction peaks of  $\text{ZrO}_2$  were evident as Zr reactant was used as 5% wt. of  $\text{TiO}_2$  in the preparation of samples. The small crystallites of  $\text{ZrO}_2$  may be dispersed over the  $\text{TiO}_2$  surface or may be located at the interstitial positions

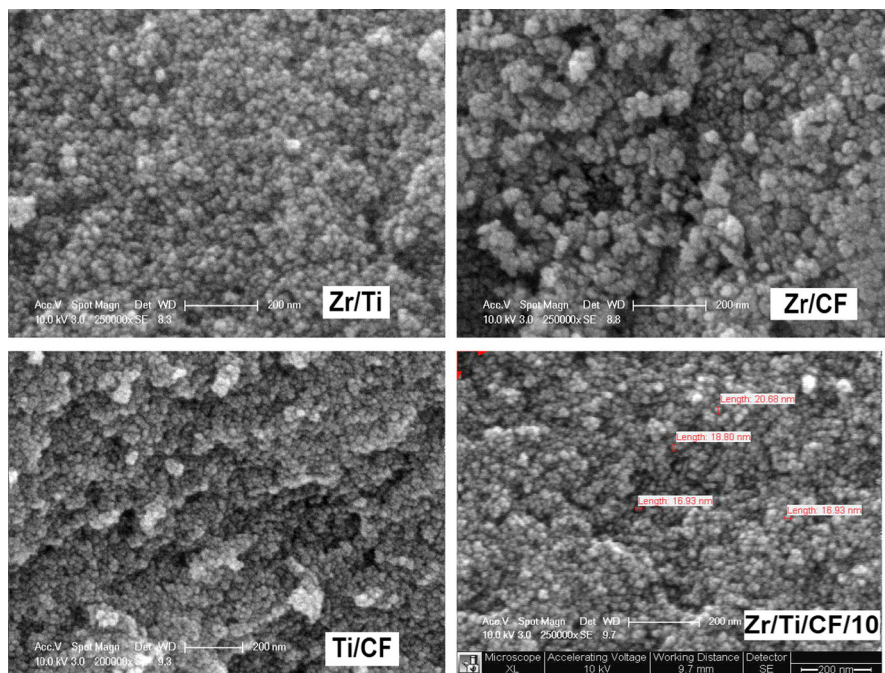


**Fig. 1** SEM images of catalysts

of  $\text{TiO}_2$ , which cannot be detected by XRD [3, 7]. The patterns of both Zr/Ti and Zr/Ti/CF/10 catalysts can be indexed to almost pure anatase  $\text{TiO}_2$  with characteristic peaks at  $25.27^\circ$ ,  $37.69^\circ$ ,  $47.98^\circ$ ,  $54.99^\circ$ ,  $62.57^\circ$  and  $70.19^\circ$ . The results indicated that the incorporation of carbon fiber did not change the crystal structure of Zr/Ti.

FTIR experiments were also performed to determine the interaction between CF and Zr/Ti and the results were depicted in Fig. S1b. The peaks at  $1730\text{ cm}^{-1}$  are ascribed to bending vibrations of adsorbed water molecules while the absorption bands detected at  $1366\text{ cm}^{-1}$  are attributed to bending  $-\text{OH}$  vibrations of Zr/Ti nanoparticles [16, 17]. Compared with Zr/Ti catalyst, the new broad band around  $3200\text{ cm}^{-1}$  appeared in the FTIR spectra of CF based catalysts indicating free hydroxyl, hydrogen bonded groups and adsorbed water molecules. The  $-\text{OH}$  stretching and  $-\text{C}-\text{OH}$  stretching bands were sensitive to the hydrogen bonding [18]. Moreover, for Zr/Ti/CF samples, the new bands at  $1600\text{ cm}^{-1}$  were assigned to the stretching vibrations of aromatic  $\text{C}=\text{C}$  ring [1]. In the spectra of pristine Zr/Ti, the low frequency bands observed at  $700\text{ cm}^{-1}$  correspond to  $\text{Ti}-\text{O}-\text{Ti}$  bonds, while the ones shifted to  $760\text{ cm}^{-1}$  are attributed to  $\text{Ti}-\text{O}-\text{C}$  bonds [1] in the spectra of Zr/Ti/CF catalysts. The formation of covalent  $\text{Ti}-\text{O}-\text{C}$  bonds revealed that Zr/Ti nanoparticles are chemically bonded to the carbon fiber rather than being adsorbed on the surface. Moreover, the existence of interfacial contact between Zr/Ti and CF results lengthening the lifetime of photo generated electron–hole pairs which enhances the photocatalytic activity [1].

UV–vis diffuse reflectance spectra of Zr/Ti, Zr/CF, Ti/CF and Zr/Ti/CF/10 catalysts are shown in Fig. S2. Absorptions of the Ti/CF and Zr/Ti/CF/10 catalysts were higher than that of Zr/Ti at visible wavelengths. The electronic structure of photocatalysts was characterized by the energy band gap ( $E_g$ ), which is essentially the energy gap between the valence band ( $E_v$ ) and the conduction band ( $E_c$ ) [19]. The  $E_g$  values of Zr/Ti, Zr/CF, Ti/CF and Zr/Ti/CF/10 were found as 2.87, 2.91, 2.76 and 2.66, respectively. The decrease in the band gap values can be ascribed to the existence of Ti–O–C bond which can accelerate the photoinduced charge transfer from  $TiO_2$  to CF, which leads to an enhancement in the photocatalytic activity of the catalyst [1].

In order to examine the surface compositions and chemical states of Zr/Ti/CF/10 heterojunction catalyst, X-ray photoelectron spectroscopy (XPS) was conducted. The catalyst has main peaks at 529 eV, 285 eV, 457 eV and 181 eV corresponding O 1s, C 1s, Ti 2p and Zr 3d chemical states (Fig. S3). In the Ti 2p spectral region, two main peaks at 457.8 eV (56.2%) and 463.5 eV (27.3%) corresponds to the Ti 2p<sub>3/2</sub> and Ti 2p<sub>1/2</sub> states, respectively. The broad peak for Ti 2p<sub>3/2</sub> suggested that the oxidation state is + 4 for the titanium present on the surface of Zr/Ti/CF/10 catalyst. The Zr 3d spectra showed two peaks with binding energies of 181.0 and 183.9 eV correspond to the Zr 3d<sub>5/2</sub> and Zr 3d<sub>3/2</sub> states, respectively.

As can be seen from O 1s spectra, the deconvolution of the O 1s band reveals oxygen bands at 529.13 and 529.7 eV corresponds to Ti–O bonds [12], whereas the bands at 528.5, 532.1 and 530.7 eV indicate O–C, OH<sup>−</sup> and O in the oxide lattice (metal–O–metal), respectively [20]. Pourbeyram et al. [21] stated that the peaks at binding energies at 530.7 eV were attributed to the oxygen form of Zr–O–H. The surface Ti–OH on the catalyst can be formed by a reaction of adsorbed H<sub>2</sub>O with TiO<sub>2</sub> ( $H_2O + Ti-O-Ti \rightarrow 2Ti-OH$ ) [12]. The surface hydroxyl groups act as electron donors for photogenerated h<sup>+</sup> and are oxidized to hydroxyl radicals ( $\bullet OH$ ), which can attack almost all organic pollutants [22]. The C 1s peaks could be deconvoluted into four major peaks with binding energies assigned at 284.2, 285.6, 284.8 and 283.6 eV originating from C=C, C–H (or C–C), C–C and C–Ti or C=O bonds [23–25]. The peak at 283.1 eV indicates the formation of O–Ti–C states.

## Photocatalytic activity measurements

### Adsorption study

The adsorption kinetics of Zr/Ti and carbon fiber based catalysts were investigated in dark with the catalyst dosage of 0.2 g/L. Fig. 2a presents the dynamic curves for the adsorption of Orange II over the catalysts. For the pristine Zr/Ti sample, the adsorption equilibrium was established within 30 min and no obvious change was observed from 120 to 180 min. Due to the presence of carbon fiber, it was clearly understood that CF based catalysts have stronger adsorption towards Orange II dye than Zr/Ti catalyst. This could be attributed to the strong  $\pi$ – $\pi$  interactions between the carbon fiber surface and dye molecules [1]. The adsorption reached equilibrium with Zr/CF and Ti/CF catalysts after 60 min of treatment. Moreover, it was also observed that with increasing CF content, the adsorption capacity also increases. At

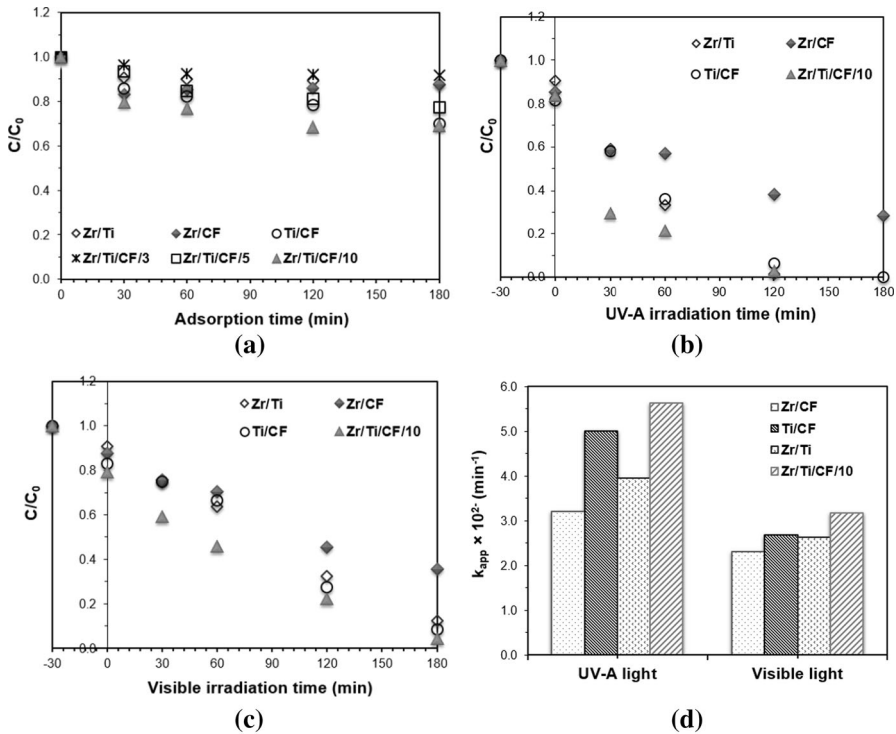


**Fig. 2** **a** Dark adsorption kinetics, **b** photodegradation under UV-A, **c** visible light irradiation and **d** the kinetic rate constants of catalysts

the end of 180 min, the adsorptive removal efficiencies of Zr/Ti/CF/3, Zr/Ti/CF/5 and Zr/Ti/CF/10 catalysts were calculated as 8.1, 22.7 and 30.8%. Zr/Ti/CF/10 catalysts was found more effective among all samples and the adsorption performance of photocatalysts towards Orange II dye molecules follows the order Zr/Ti/CF/10 > Ti/CF > Zr/Ti/CF/5 > Zr/CF > Zr/Ti/CF/3 > Zr/Ti.

*Preliminary photodegradation studies*

The photocatalytic activities of Zr/Ti, Ti/CF, Zr/CF, Zr/Ti/CF/10 catalysts were evaluated by the degradation of Orange II under UV-A and visible light illumination and the results are presented in Figs. 2b and 2c. The control Orange II dye solution in the absence of the catalyst does not exhibit the significant degradation after 180 min of UV-A light irradiation. After 120 min of UV-A light irradiation, about 98.6, 61.8, 93.6 and 97.2% of dye was diminished by Zr/Ti, Zr/CF, Ti/CF and Zr/Ti/CF/10 catalysts, respectively. The photodegradation rate was influenced by the catalyst type and Zr/Ti/CF/10 bifunctional catalyst was found more effective, which could be attributed to the dual action of photolysis and adsorption [6, 11, 12]. The carbon fibers could promote both harvesting the light and interaction between dye molecules and Zr/Ti nanoparticles. Similar phenomena were observed by other



researchers over carbonaceous based photocatalysts [1, 6, 10, 16, 19]. Singh et al. [19] stated that the increase in the degradation efficiency over composite catalyst could be due to the enhancement of the rapid separation efficiency of photo-induced electron and holes through the electronic interaction between  $\text{ZrO}_2$  and carbon structure.

The photocatalytic activity under visible light condition was examined using wavelengths between 400–800 nm. Similarly to UV-A light irradiation, the Zr/Ti/CF/10 catalyst exhibited superior catalytic performance towards the dye molecules when compared with other samples, resulting in the photodegradation of 95.8% in 3 h while that of was achieved as 87.6% by Zr/Ti. Due to the recombination issue and wide band gap, the Zr/Ti and Zr/CF samples exhibited low photocatalytic performance under visible light illumination.

The pseudo-first order kinetic model according to the *Langmuir–Hinshelwood* mechanism was applied to the photocatalytic performance of the catalysts. The kinetic model can be expressed as  $\ln(C_0/C) = k_{\text{app}} \cdot t$ , where  $k_{\text{app}}$  ( $\text{min}^{-1}$ ) is the apparent rate constant, and  $C$  and  $C_0$  are the dye concentrations at time  $t$  and at the start of the degradation, respectively. The kinetic constants calculated under UV-A light irradiation were found much higher than that of visible light (Fig. 2d). The lower photon energy in the visible region could be the reason for the lower rate values under the visible light. Moreover, the photocatalytic performance was related to the catalyst type where  $k_{\text{app}}$  values increased when carbon fiber incorporated into the structure. Under visible light, the rate constants determined for the Orange II degradation were found to be  $2.62 \times 10^{-2}$ ,  $2.31 \times 10^{-2}$ ,  $2.67 \times 10^{-2}$ , and  $3.17 \times 10^{-2} \text{ min}^{-1}$  for the Zr/Ti, Zr/CF, Ti/CF and Zr/Ti/CF/10 photocatalysts.

#### *Effect of CF concentration*

In order to verify the most favorable CF concentration in the catalyst, the photocatalytic performance of Zr/Ti/CF nanocomposites with different CF ratios were investigated under visible light irradiation after dark adsorption. As shown in Fig. 3a, it was found that the Orange II photodegradation increased with the increase of CF content in the nanocomposite catalyst. During 120 min of visible light illumination, about 61% of Orange II was photocatalytically degraded by Zr/Ti/CF/3 catalyst while that of was observed as 77.9% for Zr/Ti/CF/10 catalyst. The rate constants for Zr/Ti/CF/3, Zr/Ti/CF/5 and Zr/Ti/CF/10 were calculated as  $2.26 \times 10^{-2}$ ,  $2.81 \times 10^{-2}$  and  $3.17 \times 10^{-2} \text{ min}^{-1}$ . It could be attributed to the fact that higher content of carbon fiber can adsorb large quantities of dye molecules (shown in inset of Fig. 3a).

#### *Effect of initial concentration*

The effect of the initial solution concentration on the Orange II photodegradation was examined by varying the initial concentration from 10 to 20 mg/L and the results are illustrated in Fig. 3b. The photocatalytic decolorization of Orange II decreases as the initial concentration increases. When the initial concentration was 10 mg/L, at the end of 3 h, the photodegradation efficiency was found to be 97.7%



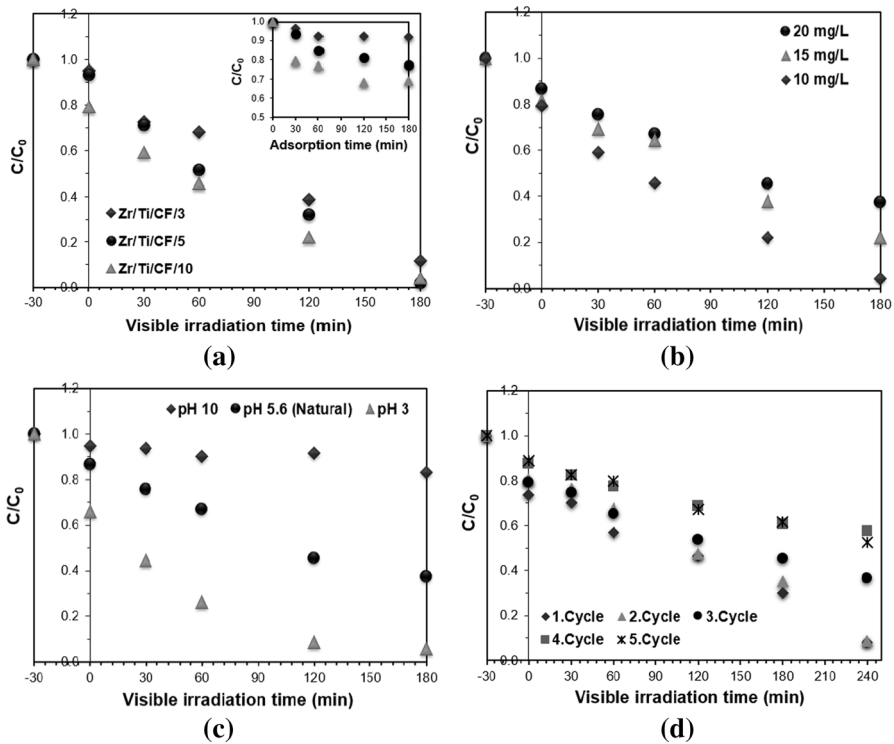


**Fig. 3** **a** Effect of CF concentration on the photodegradation, inset shows the effect of CF content on the adsorptive removal. **b** Effect of the initial solution concentration. **c** Effect of solution pH on the photocatalytic degradation by Zr/Ti/CF/10 catalyst [ $C_0$ : 20 mg/L; catalyst dose: 0.2 g/L]. **d** Reuse of the Zr/Ti/CF/10 catalyst for Orange II degradation for five cycles [ $C_0$ : 10 mg/L; catalyst dose: 0.25 g/L; natural pH]

( $k_{app} = 3.17 \times 10^{-2} \text{ min}^{-1}$ ) while that of was observed as 62.6% ( $k_{app} = 3.44 \times 10^{-2} \text{ min}^{-1}$ ) for the initial concentration of 20 mg/L. The decrease could be explained by the increase in concentration of dye molecules which block the active sites of catalyst and reduces the photons interaction. This reduction causes less absorption of the photons on the catalyst surface [26, 27]. Bassaid et al. [28] stated that the photodegradation/adsorption process is self-limited depending on the both available adsorption and photocatalytic active sites.

*Effect of pH*

As the efficiency of the photocatalytic degradation is dependent on the solution pH for the dye wastewater [29], the influence of pH on the photodegradation of Orange II was investigated at different initial pH values. As depicted by Fig. 3c, the degradation percentage of Orange II reached a maximum (94.2% at the end of 3 h) at pH 3. Moreover, when the solution pH was decreased from 5.6 to 3.0, the initial rate constant increased from  $3.44 \times 10^{-2}$  to  $5.86 \times 10^{-2} \text{ min}^{-1}$ . The catalyst

surface is positively charged in acidic media, while it is negatively charged under alkaline conditions. On the other hand, as the azo-dye molecules have two  $pK_a$  values (10.6 and 1), three different forms of Orange II could exist in the different pHs: (i) doubly protonated ( $H_2L$ ) at pH lower than 1, (ii) mono protonated ( $HL^-$ ) in the pH range between 1 and 10.6 and (iii) nonprotonated ( $L^{2-}$ ) at pH above 10.6, where  $L^{2-}$  is the Orange II molecule in the following form  $C_{16}H_{11}N_2OSO_3^{2-}$  [30]. Thus, the protonation effect greatly favored the adsorption of Orange II anions via electrostatic forces at lower pH values [29]. Under acidic conditions, the catalyst surface is protonated and becomes positively charged ( $-COOH_2^+$ ). Negatively charged Orange II dye ( $HL^-$ ) is adsorbed on the catalyst surface by electrostatic attractions. In contrast, the surface is deprotonated and becomes negatively charged ( $-COO^-$ ) in basic medium. Due to the Coulombic repulsion, the adsorption of Orange II molecules on the Zr/Ti/CF/10 catalyst surface decreases. The pH was adjusted by NaOH solution for higher pH values. Therefore,  $OH^-$  formation in the solution also increases and competition occurs between the negatively charged dye molecule and  $OH^-$  ions for the adsorption on the surface, which also reduces the photocatalytic activity [31]. Therefore, the optimal pH was found as 3 for this reaction system. Similar phenomena were observed by other researchers [32, 33].

### *Stability experiments*

The re-use performance of Zr/Ti/CF/10 catalyst was examined for Orange II removal for consecutive five-run reactions under visible light irradiation. As shown in Fig. 3d, the photocatalytic decolorization percentage was not significantly varied till three cycle, after that the degradation efficiency decreased from 92 to 47% after reusing fifth cycles as compared to first cycle.

## **Conclusions**

Zr/Ti/CFs composite catalysts were prepared via in situ process by solvothermal method. The X-ray diffraction patterns varied with strong peaks of anatase phase for the composite catalyst. FTIR and XPS measurements suggested the formation of covalent Ti–O–C bonds revealed that Zr/Ti nanoparticles are chemically bonded to the carbon fiber rather than being adsorbed on the surface. The Zr/Ti/CFs exhibited higher photocatalytic activity than that of Zr/Ti, Zr/CF and Ti/CF catalysts under UV-A and visible light irradiation. The remarkable photocatalytic efficiency of the Zr/Ti/CF/10 photocatalyst was attributed to the reduced band gap, synergetic effect of adsorption–photocatalysis, and decreased electron–hole recombination rate due to trapping of electrons from the conduction band by CF.

**Acknowledgements** The authors are grateful to Yalova University for financial support.

## References

1. Prabhakarrao N, Ravi Chandra M, Siva Rao T (2017) *J Alloys Compd* 694:596–606
2. Isleyen I, Ilkme ES, Pozan Soylu GS (2017) *Korean J Chem Eng.* <https://doi.org/10.1007/s11814-017-0065-6>
3. Tokmakci T, Ozturk A, Park J (2013) *Ceram Int* 39:5893–5899
4. Bilgin Simsek E (2017) *Appl Catal B* 200:309–322
5. Rani S, Aggarwal M, Kumar M, Sharma S, Kumar D (2016) *Water Sci* 30:51–60
6. Oh WC, Zhang FJ, Chen ML, Lee YM, Ko WB (2009) *J Ind Eng Chem* 15:190–195
7. Song S, Hong F, He Z, Wang H, Xu X, Chen J (2011) *Appl Surf Sci* 257:10101–10108
8. Gao B, Lim TM, Subagio DP, Lim TT (2010) *Appl Catal A* 375:107–115
9. Liu H, Liu G, Zhou Q (2009) *J Solid State Chem* 182:3238–3242
10. Shi JW (2009) *Chem Eng J* 151:241–246
11. Wang Z, Yoshinaga K, Bu XR, Zhang M (2015) *J Hazard Mater* 290:134–141
12. Li Y, Liu C, Xu P, Li M, Zen M, Tang S (2014) *Chem Eng J* 243:108–116
13. Dey NK, Kim MJ, Kim KD, Seo HO, Kim D, Kim YD, Lim DC, Lee KH (2011) *J Mol Catal A* 337(1–2):33–38
14. Wang T, Li Y, Qu G, Liang D, Hu S (2016) *Water Air Soil Pollut* 227:464
15. Bilgin Simsek E, Novak I, Sausa O, Berek D (2017) *Res Chem Intermed* 43:503–522
16. Anku WW, Oppong SOB, Shukla SK, Agorku ES, Govender PP (2016) *Prog Nat Sci* 26:354–361
17. Cho DW, Jeon BH, Jeong Y, Nam IH, Choi UK, Kumar R, Song H (2016) *Appl Surf Sci* 372:13–19
18. An Y, Han W, Han J, Zhao G, Zhou S, Zhang X (2016) *Mater Des* 112:275–281
19. Singh BR, Shoeb M, Khan W, Naqvi AH (2015) *J Alloys Compd* 651:598–607
20. Zhao D, He Z, Wang G, Wang H, Zhang Q, Li Y (2016) *J Colloid Interface Sci* 478:227–235
21. Pourbeyram S, Alizadeh S, Gholizadeh S (2016) *J Environ Chem Eng* 4:4366–4373
22. Guo WX, Zhang F, Lin CJ, Wang ZL (2012) *Adv Mater* 24(35):4761–4764
23. Wu G, Ma L, Wang Y, Liu L, Huang Y (2016) *Composites Part A* 84:1–8
24. Sarac AS, Serantoni M, Tofail SAM, Henry J, Cunnane V, McMonagle JB (2005) *Appl Surf Sci* 243:183–198
25. Singh B, Fang Y, Cowie BCC, Thomsen L (2014) *Org Geochem* 77:1–10
26. Bechambi O, Sayadi S, Najjar W (2015) *J Ind Eng Chem* 32:201–210
27. Sin JC, Lam SM, Lee KT, Mohamed AR (2013) *J Colloid Interface Sci* 401:40–49
28. Bassaid S, Bellal B, Trari M (2015) *Reac Kinet Mech Cat* 115:389–400
29. Li G, Qu J, Zhang X, Liu H, Liu H (2006) *J Mol Catal A* 259:238–244
30. Abramian L, El-Rassy H (2009) *Chem Eng J* 150:403–410
31. Sin JC, Lam SM, Lee KT, Mohamed AR (2013) *J Colloid Interface Sci* 401:40–49
32. Laipan M, Zhu R, Zhu J, He H (2016) *J Mol Catal A* 415:9–16
33. Zhou G, Guo J, Zhou G, Wan X, Shi H (2016) *J Environ Sci* 47:63–70